High-precision and fast computation of Jacobi–Fourier moments for image description

C. Camacho-Bello,[1,*] C. Toxqui-Quitl,[2] A. Padilla-Vivanco,[2] and J. J. Báez-Rojas[1]

[1]*Instituto Nacional de Astrofísica, Óptica y Electrónica, Luis Enrique Erro No. 1, 72840, Puebla, Mexico*
[2]*Universidad Politécnica de Tulancingo, Ingenierías No. 100, 43629, Hidalgo, Mexico*
**Corresponding author: joel_camacho@inaoep.mx*

Received June 13, 2013; revised November 21, 2013; accepted November 26, 2013;
posted November 27, 2013 (Doc. ID 192152); published December 16, 2013

A high-precision and fast algorithm for computation of Jacobi–Fourier moments (JFMs) is presented. A fast recursive method is developed for the radial polynomials that occur in the kernel function of the JFMs. The proposed method is numerically stable and very fast in comparison with the conventional direct method. Moreover, the algorithm is suitable for computation of the JFMs of the highest orders. The JFMs are generic expressions to generate orthogonal moments changing the parameters α and β of Jacobi polynomials. The quality of the description of the proposed method with α and β parameters known is studied. Also, a search is performed of the best parameters, α and β, which significantly improves the quality of the reconstructed image and recognition. Experiments are performed on standard test images with various sets of JFMs to prove the superiority of the proposed method in comparison with the direct method. Furthermore, the proposed method is compared with other existing methods in terms of speed and accuracy.

OCIS codes: (100.0100) Image processing; (100.2960) Image analysis; (150.0150) Machine vision; (100.4994) Pattern recognition, image transforms; (100.5760) Rotation-invariant pattern recognition.
http://dx.doi.org/10.1364/JOSAA.31.000124

1. INTRODUCTION

Jacobi–Fourier moments (JFMs) are widely used in image analysis, pattern recognition, and machine vision applications. They were first introduced to image analysis by Ping *et al.* [1]. The most significant property of JFMs is their ability to characterize, evaluate, and manipulate visual information with minimum redundant information. They also have the property of being invariant to translation, rotation, and scale. Moreover, the variation of parameters α and β of the Jacobi polynomials can produce different sets of orthogonal moments: orthogonal Fourier–Mellin moments ($\alpha = 2, \beta = 2$), Chebyshev–Fourier moments ($\alpha = 2, \beta = (3/2)$), pseudo-Jacobi–Fourier moments ($\alpha = 4, \beta = 3$), and Legendre–Fourier Moments ($\alpha = 1, \beta = 1$). In image analysis and pattern recognition, JFMs have been used in classification of microcalcification in mammograms [2], classification of mechanical parts [3], and gait recognition [4].

Teague [5] suggested reconstruction of a digital image from orthogonal moments and introduced the Zernike moments. The reconstruction helps us to know how well an image can be described with a finite number of moments; it is also associated with the quality of the description and the invariance. There is a lot of literature on image analysis, including the reconstruction of digital images [6–11]. This analysis only performs the reconstruction of binary objects, such as ideograms, and letters. Padilla *et al.* [12] present a detailed analysis of the reconstruction of gray-level images using four different families of orthogonal moments: Zernike, orthogonal Fourier–Mellin, Chebyshev–Fourier, and pseudo-Jacobi–Fourier moments. In a previous analysis, two types of errors occurred in the direct calculation of orthogonal moments: geometric error and numerical integration error [13]. Such errors contribute significantly to the inaccuracy of orthogonal moments and reconstruction. Recently, Xin *et al.* [14] proposed an algorithm for high-precision numerical computation of Zernike moments to significantly improve the quality of the reconstructed image. The authors propose reconfiguring the square pixel array to an array of polar pixels to eliminate errors of geometry and to be able to calculate the integral analytically. Moreover, Wee and Paramesra [15] achieve the minimization of geometry error through a circular mapping, where a whole square image is mapped inside a unit disk and the integral is calculated analytically, similar to the exact geometric moments. However, this method is numerically unstable for orders greater than 50. To reduce the computational time, a few algorithms have been proposed to speed up the computation of orthogonal moments [16–19]. These methods suggest recursive algorithms to estimate the coefficients of the radial polynomials. It has been observed that the calculation of higher-order polynomials using radial-expression-based recursive estimation of the coefficients causes numerical instability; this is due to the use of power in radial coordinates [20].

In this work, we present a novel algorithm to compute JFMs in a fast and high-precision way, based on the polar pixel arrangement scheme and recurrence relation with respect to n, which is free powers of r. This new recurrence relation helps us to calculate faster and reduces numerical instability in higher-order radial polynomials. The polar pixel arrangement scheme eliminates geometric and numerical integration errors. Moreover, this study proposes the search for optimal parameters α and β of JFMs to significantly improve the quality of reconstruction of a standard test image.

This work is organized as follows: Section 2 gives a brief review of JFMs. A recursive method for the fast computation of the Jacobi polynomials is presented in Section 3. Section 4 gives a detailed description of the polar pixel arrangement scheme and the image conversion via interpolation bicubic for the high-precision computing of JFMs. Empirical evaluation of accurate and fast computation of the JFMs is presented in Section 5. Finally, some conclusions are presented in Section 6. The recurrence relationship between Jacobi and Zernike polynomials is shown in the Appendix A.

2. REVIEW OF JACOBI–FOURIER MOMENTS

The general expression for JFMs of order n and repetition m, for a given image function $f(r,\theta)$ in polar coordinates, is given by

$$A_{n,m} = \int_0^{2\pi}\int_0^1 f(r,\theta)P_{nm}(r,\theta)r\mathrm{d}r\mathrm{d}\theta, \tag{1}$$

where $P_{nm}(r,\theta)$ is the kernel function that consists of two separable functions sets: the Jacobi orthogonal polynomial $J_n(\alpha,\beta,r)$ and the exponential Fourier factor $\exp(jm\theta)$, expressed by

$$P_{nm}(r,\theta) = J_n(\alpha,\beta,r)\exp(jm\theta). \tag{2}$$

The radial orthonormal Jacobi polynomials are defined as

$$J_n(\alpha,\beta,r) = \sqrt{\frac{w(\alpha,\beta,r)}{b_n(\alpha,\beta)}}G_n(\alpha,\beta,r), \tag{3}$$

where $G_n(\alpha,\beta,r)$ are the Jacobi polynomials, $b_n(\alpha,\beta)$ is the normalization constant, and $w(\alpha,\beta,r)$ is the weight function [21]. These expressions are calculated as follows [22]:

$$G_n(\alpha,\beta,r) = \frac{n!\Gamma(\beta)}{\Gamma(\alpha+n)}\times\sum_{s=0}^{n}(-1)^s\frac{\Gamma(\alpha+n+s)}{(n-s)!s!\Gamma(\beta+s)}r^s, \tag{4}$$

$$b_n(\alpha,\beta) = \frac{n!\Gamma^2(\beta)\Gamma(\alpha-\beta+n+1)}{\Gamma(\beta+n)\Gamma(\alpha+n)(\alpha+2n)}, \tag{5}$$

$$w(\alpha,\beta,r) = (1-r)^{\alpha-\beta}r^{\beta-1}, \tag{6}$$

where $\Gamma(\cdot)$ is the gamma function, $\alpha-\beta>-1$, and $\beta>0$.

For digital images, Eq. (1) cannot be directly applied. Let $f(r_{i,j},\theta_{i,j})$ be a digital image with spatial dimensions $M\times N$. Its discrete moments $A_{n,m}$ are given by

$$\tilde{A}_{n,m} = \sum_{i=0}^{M-1}\sum_{j=0}^{N-1}f(r_{i,j},\theta_{i,j})\tilde{P}_{nm}(r_{i,j},\theta_{i,j}), \tag{7}$$

where the discrete polar coordinates are expressed by

$$r_{i,j} = \sqrt{x_i^2+y_j^2} \qquad r_{i,j}\le 1,$$
$$\theta_{i,j} = \arctan\left(\frac{y_j}{x_i}\right), \tag{8}$$

and they are transformed by

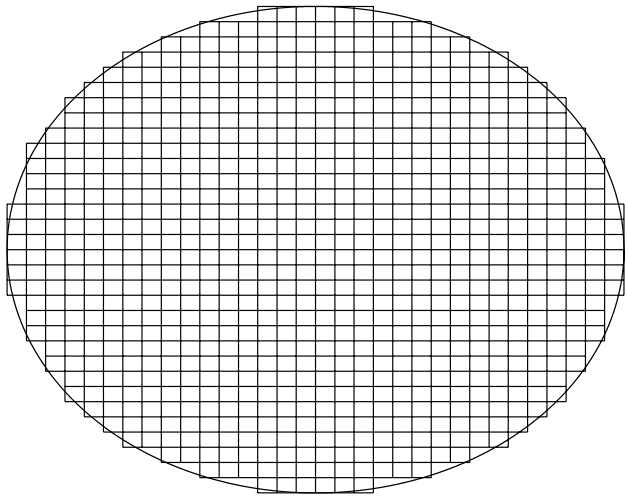

Fig. 1. Cartesian pixel region for computing JFMs.

$$x_i = -1+\frac{2i}{N-1}, \qquad y_j = -1+\frac{2j}{M-1}, \tag{9}$$

where $i=0,\ldots,N-1$, and $j=0,\ldots,M-1$. When the integrals of Eq. (1) are replaced by summations and the image is normalized inside the unit disk, this approach is known as zeroth-order approximation or direct method.

The accuracy of JFMs computed by Eq. (7) suffers from two sources of error. First, geometric error exists due to the fact that the total area covered by all the square pixels involved in the computation of moments is not exactly the unit disk, as illustrated by the ragged border in Fig. 1, and the second error is caused by an approximation of the integral of Eq. (1) [13]. In Section 4, these two errors are reduced by implementing polar pixels to facilitate the computation of the integral.

3. PROPOSED RECURSIVE METHOD FOR THE FAST COMPUTATION OF JACOBI–FOURIER MOMENTS

Owing to the very time-consuming nature of computing the polynomial values using Eq. (3), we propose a recursive method for the fast computation of the Jacobi polynomials of order n, occurring in the kernel function of JFMs. Furthermore, changing the parameters α and β of the recurrence relations generated different families of orthogonal polynomials with less computation time.

The calculation of factorials in Eq. (3) increases the computation time and it is only accurate for factorials less than 21; it is accurate for the first 15 digits of double precision numbers. Moreover, the computation of the nth power of r in higher orders cause numerical instability in values around 1 in the unit disc. Consequently, the numerical instability will drastically affect the quality of image reconstruction, particularly for large images (larger than 128×128 pixels). The same problems also occur for orthogonal Fourier–Mellin moments [20]. In this case, the relation recurrence of the orthogonal polynomials eliminates the factorial calculation and powers of r. However, a relation recurrence for the computation of JFMs has not been presented yet. We propose the recurrence relation with respect to n for the computing of Jacobi polynomials, which is given by

$$D_n J_n(\alpha,\beta,r) = (C_{n-1} + 1 - 2r)J_{n-1}(\alpha,\beta,r) - D_{n-1}J_{n-2}(\alpha,\beta,r), \tag{10}$$

where $r \in [0,1]$, $\alpha - \beta > -1$, $\beta > 0$ and the coefficients C_n and D_n are calculated as follows:

$$C_n = \frac{(\alpha-1)(2\beta-\alpha-1)}{(2n+\alpha-1)(2(n-1)+\alpha-1)}, \tag{11}$$

$$D_n = \sqrt{\frac{4n(n+\alpha-\beta)(n+\beta-1)(n+\alpha-1)}{(2n+\alpha-1)^2(2n+\alpha)(2n+\alpha-2)}}. \tag{12}$$

For the initial numerical calculation, the Jacobi polynomials of the zeroth and first normalized orders are given by

$$J_0(\alpha,\beta,r) = \sqrt{\frac{w(\alpha,\beta,r)}{b_0(\alpha,\beta)}}, \tag{13}$$

$$J_1(\alpha,\beta,r) = J_0(\alpha,\beta,r)\sqrt{\frac{(\alpha+2)\beta}{\alpha-\beta+1}}\left(1 - \frac{\alpha+1}{\beta}r\right). \tag{14}$$

It is clear that the recurrence relation by Eq. (10) is free from factorial terms and powers of r; for these reasons, it is reduced from numerical instability and behaves significantly better than the direct method. In the conventional method, numerical instability starts for orders ≥21. Figure 2 shows the results of calculating the Jacobi polynomials by Eqs. (3) and (10), proposed here with different values of α and β: Fig. 2(a) shows the plot of the Zernike polynomial for order $n = 46$ and $m = 0$, Fig. 2(b) shows the plot of the Mellin polynomial for order $n = 23$, and Fig. 2(c) shows the plot of Chebyshev polynomial for order $n = 23$. The recurrence relation for Jacobi polynomials is very stable for higher orders.

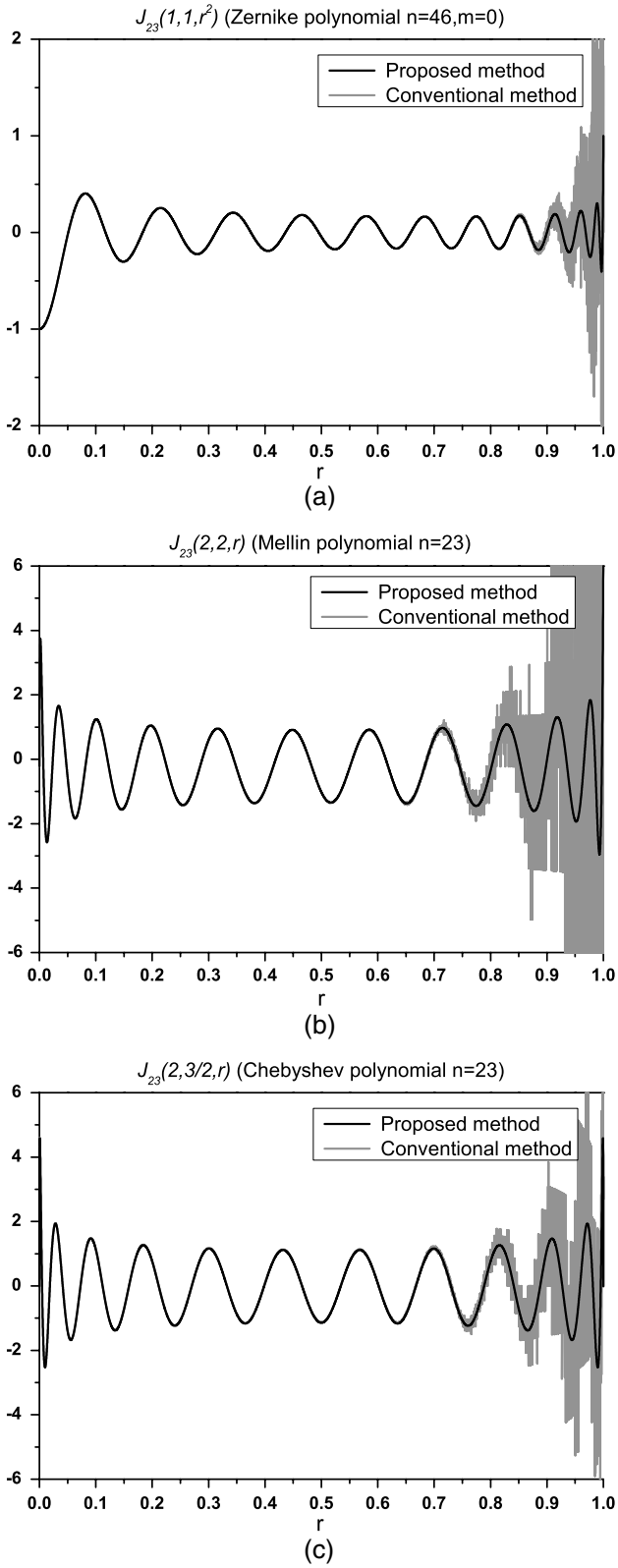

Fig. 2. Graphs of Jacobi polynomials of order $n = 23$ through the conventional method and the recurrence relation. (a) $J_{23}(1,1,r^2)$, (b) $J_{23}(2,2,r)$, and (c) $J_{23}(2,3/2,r)$.

4. HIGH-PRECISION COMPUTATION OF JACOBI–FOURIER MOMENTS

In order to increase the numerical accuracy calculation, Xin *et al.* [14] proposed an algorithm based on changing the shape of the square pixels in a polar pixel scheme for Zernike moments; this same strategy is used here to compute the JFMs. This section presents an algorithm for computing JFMs in a tiling scheme of polar pixels, which reduces both the geometric and the integration error.

A. Computing Jacobi–Fourier Moments in Polar Pixels

Computation of orthogonal moments in polar pixels is based on the idea of a pixel arrangement scheme as shown in Fig. 3. The unit disk is uniformly divided along the radial direction into U sections, with radial distance of $r_u = u/U$ where $u = 1 \ldots U$. The number of polar pixels in the uth ring is $S_u = (2u-1)V$, with angles $\theta_{uv} = (v-1)2\pi/S_u$, where $v = 1 \ldots S_u$ and V is the number of sectors contained in the innermost section. The total number of polar pixels is VU^2 and each of them has an area of π/VU^2. In practice, Xin *et al.* [14] recommended setting a value of $V = 4$ and $N/2 \le U \le N$ for a $N \times N$ image.

The calculation of the JFMs is performed by summation of all sectors inside the unit disk. Equation (1) for the calculation of JFMs is rewritten as

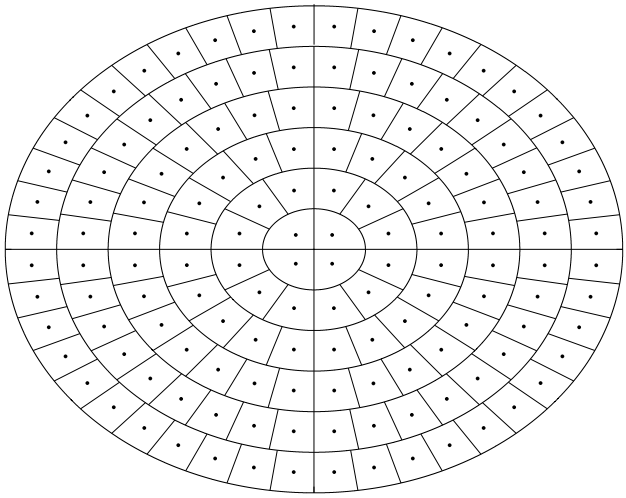

Fig. 3. Polar pixel representation of an image.

$$\hat{A}_{nm} = \sum_{u=1}^{U} \sum_{v=1}^{(2u-1)V} \hat{f}(r_{uv}, \theta_{uv}) \omega_{nm}(r_{uv}, \theta_{uv}), \tag{15}$$

where $\hat{f}(r_{uv}, \theta_{uv})$ is an approximation of the function $f(r_{ij}, \theta_{ij})$ defined over a set of concentric sectors Ω_{uv}, and the factor $\omega_{nm}(r_{uv}, \theta_{uv})$ is given by

$$\begin{aligned} \omega_{nm}(r_{uv}, \theta_{uv}) &= \iint_{\Omega_{uv}} J_n(\alpha, \beta, r) \exp(jm\theta) r \mathrm{d}r \mathrm{d}\theta, \\ &= \int_{r_{uv}^{(s)}}^{r_{uv}^{(e)}} J_n(\alpha, \beta, r) r \mathrm{d}r \int_{\theta_{uv}^{(s)}}^{\theta_{uv}^{(e)}} \exp(jm\theta) \mathrm{d}\theta, \\ &= I_1 \times I_2, \end{aligned} \tag{16}$$

where $r_{uv}^{(s)}$ and $r_{uv}^{(e)}$ denote the starting and ending radii of the sector Ω_{uv}, respectively, while $\theta_{uv}^{(s)}$ and $\theta_{uv}^{(e)}$ denote the starting and ending angles of the sector Ω_{uv}, respectively, as shown in Fig. 4. The integral of the complex Fourier component of Eq. (16) can be analytically calculated as

$$I_2 = \begin{cases} \frac{j}{m}[\exp(-jm\theta_{uv}^{(e)}) - \exp(-jm\theta_{uv}^{(s)})], & m \neq 0 \\ \theta_{uv}^{(e)} - \theta_{uv}^{(s)}, & m = 0 \end{cases}. \tag{17}$$

Moreover, the analytical calculation of the integral over the coefficients of the orthonormal Jacobi polynomials is numerically unstable in computation of powers greater than 21 for the radial coordinate, causing an increase of the error in the calculation of JFMs. This error can be reduced by the recurrence relation given in Section 3. Therefore, we chose to

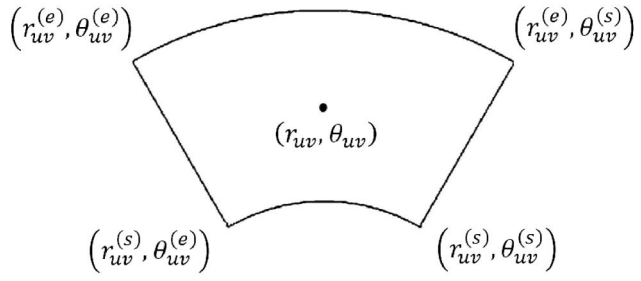

Fig. 4. Concentric sector Ω_{uv} or polar pixel.

Table 1. Weights (η_k) and Location of Sampling Points (z_k) for 10-Point Gaussian Quadrature

k	η_k	z_k
1	0.0666713443	−0.9739065285
2	0.1494513492	−0.8650633667
3	0.2190863625	−0.6794095683
4	0.2692667193	−0.4333953941
5	0.2955242247	−0.1488743390
6	0.2955242247	0.1488743390
7	0.2692667193	0.4333953941
8	0.2190863625	0.6794095683
9	0.1494513492	0.8650633667
10	0.0666713443	0.9739065285

compute the integral using the 10-point Gaussian quadrature rule, which is less accurate but stable numerically, to compute integrals of higher-order polynomials. The composite Gaussian quadrature rule for numerical integration of the Jacobi polynomial can be stated as

$$I_1 = \frac{r_{uv}^{(e)} - r_{uv}^{(s)}}{2} \sum_{k=1}^{10} \eta_k J_n\left(\alpha, \beta, \frac{r_{uv}^{(e)} - r_{uv}^{(s)}}{2} z_k + \frac{r_{uv}^{(e)} + r_{uv}^{(s)}}{2}\right). \tag{18}$$

Here, η_k are weights and $z_k \in [-1, 1]$ are the points where the function is evaluated. The values of η_k and z_k are given in Table 1. It is clear that the 10-point Gaussian quadrature rule requires greater computation time for the number of points that it is needed, but the polar pixel arrangement reduces the complexity of two-dimensional to one-dimensional integrals; this characteristic is not reached with square pixels. The two-dimensional method of Gaussian quadrature is used for the exact calculation of orthogonal moments [23,24]. The algorithm is computationally more expensive, as the kernel function is evaluated in k^2 points while the one-dimensional integral only required k points.

B. Image Representation

A digital image is defined by sets of square pixels. It can be easily verified that the locations of the Cartesian pixels do not coincide with those of the polar pixels, as shown in Fig. 3. Therefore, we have to derive the polar counterpart of a given pixel Cartesian image before computing the Jacobi–Fourier moments. This problem can be resolved by bicubic interpolation of the third order introduced in [25]. Cubic convolution interpolation is a new technique for resampling discrete data. The cubic convolution interpolation kernel is given by

$$u(x) = \begin{cases} \frac{3}{2}|x|^3 - \frac{5}{2}|x|^2 + 1 & 0 < |x| < 1 \\ -\frac{1}{2}|x|^3 + \frac{5}{2}|x|^2 - 4|x| + 2 & 1 < |x| < 2 \\ 0 & 2 < |x| \end{cases}. \tag{19}$$

The image value at Ω_{uv} can be estimated via the two-dimensional cubic convolution interpolation function; this function is expressed by

$$\hat{f}(r_{uv}, \theta_{uv}) = \sum_{i=k-1}^{k+2} \sum_{j=l-1}^{l+2} f(i,j) u(k-i) u(l-j), \tag{20}$$

where u is the interpolation kernel of Eq. (19), $k = (N/2)r_{uv}\cos\theta_{uv} + (N/2) + 1$, and $l = (N/2)r_{uv}\sin\theta_{uv} + (N/2) + 1$. Figure 5 shows the boat image represented in a polar pixel scheme with the parameters $V = 4$ and $U = 32$. The polar pixel values were obtained by bicubic interpolation of Eq. (20).

5. VALUATION OF THE ALGORITHM

There are a few results in the literature showing reconstructions of images greater than or equal to 128×128 pixels with high orders [14,20,26]. This section performs the evaluation of the proposed method from two different perspectives, a 256×256 pixel image reconstruction and invariance to rotation and scale. Furthermore, a comparative analysis of the normalization image reconstruction error (NIRE) and the computation time for different methods is performed.

The test images are shown in Fig. 6. The boat image has fine details, such as pulleys, ropes, masts, and antennas that hinder reconstruction and can be used to visually verify reconstruction quality. Moreover, the errors inherent in the estimation of the JFMs are caused by numerical instability when calculating Jacobi polynomials, the geometry of the pixels, and the approximation of the integral. These errors are affected in the same way in binary and gray-level images. The proposed method significantly reduces these errors so that the fine details of the image are observed in the reconstructed image.

A. Improvement of Image Reconstruction

Image reconstruction can help to determine how well an image may be characterized by a small finite set of its moments. According to orthogonal theories, an original image $f(i,j)$ can be reconstructed by an infinite number of Jacobi–Fourier moments. The reconstructed discrete distribution of the image is given by

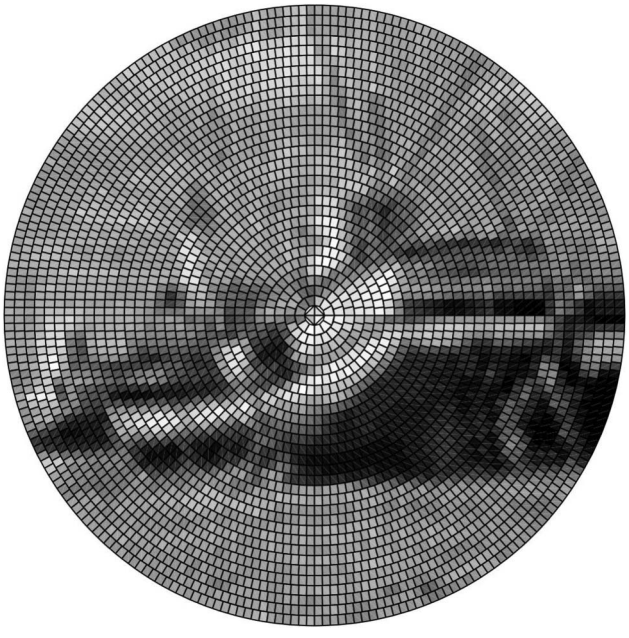

Fig. 5. Boat image in a polar pixel scheme.

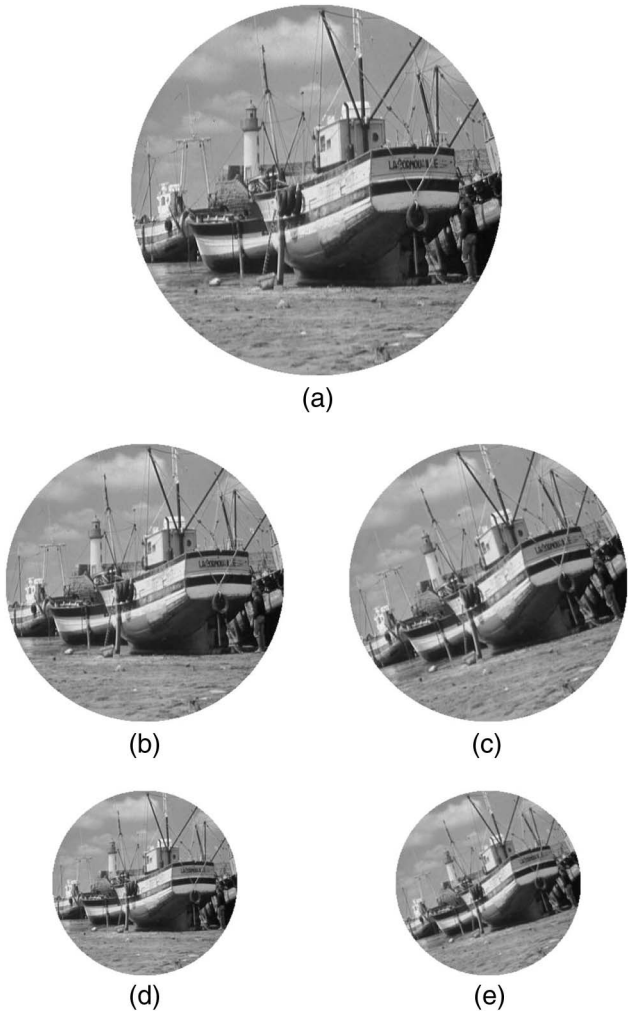

Fig. 6. Boat image for different scales and rotations. (a) Original 512×512 pixel test image. (b) The image in (a) is scaled by $k = 0.75$. (c) The image in (a) is scaled by $k = 0.75$ and rotated by $g = 15°$. (d) The image in (a) is scaled by $k = 0.50$. (e) The image in (a) is scaled by $k = 0.50$ and rotated by $g = 15°$.

$$\tilde{f}(i,j) = \sum_{n=0}^{L}\sum_{m=0}^{L} |\hat{A}_{nm}| J_n(\alpha,\beta,r_{ij}) \exp(-jm\theta_{ij}), \tag{21}$$

where $\tilde{f}(i,j)$ is the reconstructed version of $f(i,j)$, and L is the maximum order of JFMs used in the reconstruction of the image. The JFMs are a generic expression to generate different sets of orthogonal moments and, in addition, the low computational cost allows extensive analysis. Therefore, digital image reconstruction is performed for a set of orthogonal moments based on the JFMs. In the analysis of reconstruction of gray-level images, Zernike moments (ZMs) [5], orthogonal Fourier–Mellin moments (OFMMs) [6], pseudo-Jacobi–Fourier moments (PJFMs) [7], Chebyshev–Fourier moments (CFMs) [8], Legendre–Fourier moments (LFMs), and JFMs ($\alpha = 8$, $\beta = 2$) are used, as shown in Figs. 7 and 8. In all of the cases, the reconstructions performed by the proposed method are visually much better than those performed by the direct method. There is a particular case of ZMs for low order, as shown in Fig. 7, where $L = 20$; they are visually identical. In the case of the direct method, the image is obscured as the orders are increased. This is because of an error,

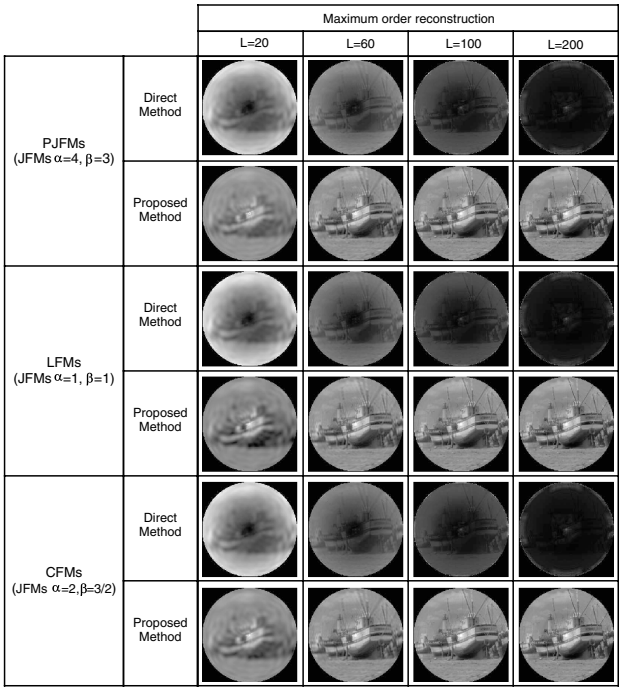

Fig. 7. 256×256 pixel reconstructions of the image in Fig. 4(d) using pseudo-Jacobi–Fourier moments, Legendre–Fourier moments, and Chebyshev–Fourier moments. The maximum orders of reconstruction are 20, 100, and 200.

which is demonstrated in Eq. (1), that causes an error in the orthogonality condition when it is reconstructed.

The NIRE is used for the performance analysis of orthogonal moments [6]. It is defined as the normalized mean square error between the input image $f(i,j)$ and its reconstruction $\tilde{f}(i,j)$, and in discrete form is given by

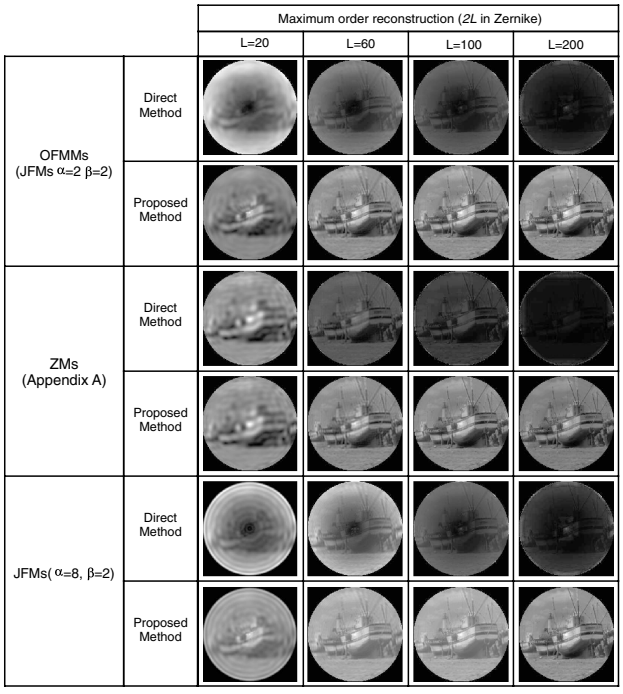

Fig. 8. 256×256 pixel reconstructions of the image in Fig. 4(d) using orthogonal Fourier–Mellin moments, ZMs, and JFMs with $\alpha = 8$ and $\beta = 2$. The maximum orders of reconstruction are 20, 60, 100, and 200.

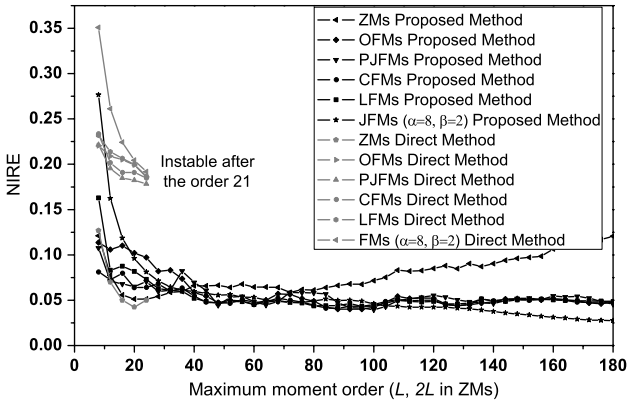

Fig. 9. NIRE of the 256×256 pixel boat image for different orthogonal moments.

$$\mathrm{NIRE} = \frac{\sum_{i=0}^{N-1}\sum_{j=0}^{M-1}[\tilde{f}(i,j) - f(i,j)]^2}{\sum_{i=0}^{N-1}\sum_{j=0}^{M-1} f^2(i,j)}. \tag{22}$$

The NIRE results for the different sets of orthogonal moments (PJFMs, LFMs, CFMs, OFMMs, ZMs, and JFMs), using the direct method and proposed method, are shown in Fig. 9. The quality of reconstruction by the proposed method is significantly better than the direct method. In the proposed method, the reconstruction quality remains stable to $n > 100$, while in the direct method, the NIRE decreases to a given point and then increases.

Bhatia and Wolf [27] pointed out that there is an infinite number of complete sets of orthogonal polynomials that are invariant to rotation and can be obtained from the Jacobi polynomials. Each set is obtained by the combination of the parameters α and β. Therefore, there may be a set of orthogonal moments better fit to specific applications. We define the mean of NIRE as a metric to quantitatively evaluate the best combinations of α and β. The mean value of NIRE is given by

$$\Psi(\alpha,\beta) = \frac{1}{p}\sum_{L=1}^{p} \mathrm{NIRE}(L,\alpha,\beta), \tag{23}$$

where L is the maximum order of JFMs used in the reconstruction of the input image and p is the cutting orders. The cutting order p can find the optimal parameters for moments of low and high order. In general, low-order moments represent the global shape of an image, and high-order moments represent the detail [12]. Figure 10 shows the exhaustive searches performed for the boat image [Fig. 6(d)] for values of $\alpha = 1\ldots10$ and $\beta = 1\ldots10$, with the aim to find the optimum combination of moments of low and high order. Note that the search space is restricted by $\alpha - \beta > -1$, and the sections with minimum values represent the neighborhood of the best combinations of α and β. In the case of low-order moments, the optimum parameters, $\alpha = 2$ and $\beta = 1$, are found as shown in Fig. 10(a); similarly are the high-order moments, $\alpha = 8$ and $\beta = 2$, shown in Fig. 10(b). For the latter, the results of the reconstruction and NIRE are, respectively, shown in Figs. 8 and 9. The fast calculation proposed of the JFM facilitates the search for the best values α and β of the moments of low and high orders that best fit specific applications.

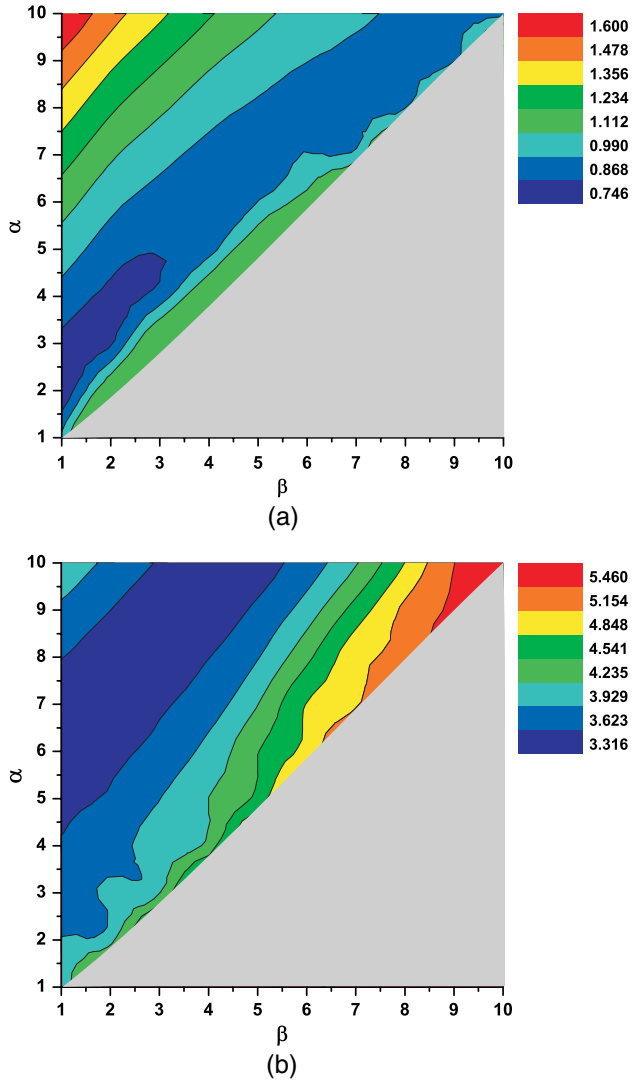

Fig. 10. Search space of the optimal parameters. (a) Low-order moments, $L = 20$. (b) High-order moments, $L = 200$.

B. Improvement of Rotation and Scale Invariance of JFMs

One of the most important properties of the orthogonal moments in the unit disk is the invariant representation of the scaled and rotated object. If a distorted image $f(r/k, \theta - \gamma)$ is rotated γ degrees and scaled by a factor k, all JFMs of the resulting image, $\hat{A}_{nm}^{(\gamma,k)}$, are related with the JFMs of the original image by

$$\hat{A}_{nm}^{(\gamma,k)} = \hat{A}_{nm} e^{-im\gamma}. \tag{24}$$

Therefore, the modulus JFMs,

$$|\hat{A}_{nm}^{(\gamma,k)}| = |\hat{A}_{nm}|, \tag{25}$$

are invariant to scale and rotation. In the accurate calculation, it is not required that Eq. (25) be normalized such as in the direct method. The normalization for the JFMs proposed by Ping *et al.* [1] is given as

$$\frac{1}{k^2}|\hat{A}_{nm}^{(\gamma,k)}| = |\hat{A}_{nm}|, \tag{26}$$

where k is obtained using the low orders of Fourier–Mellin moments [6]

$$M_{nm} = \int_0^{2\pi}\int_0^1 r^n f(r/k, \theta - \gamma)\exp(-im\theta) r\,dr\,d\theta, \tag{27}$$

$$\hat{M}_{nm} = \int_0^{2\pi}\int_0^1 r^n f(r, \theta)\exp(-im\theta) r\,dr\,d\theta, \tag{28}$$

$$k = \frac{[M_{10}/M_{00}]}{[\hat{M}_{10}/\hat{M}_{00}]}. \tag{29}$$

The change of magnitude of JFMs before and after the image will be rotated and scaled reveals its computational accuracy. The relative error of the magnitude of JFMs is given by

$$\delta A_{nm} = \frac{\frac{1}{k^2}|\hat{A}_{nm}^{(\gamma,k)}| - |\hat{A}_{nm}|}{|\hat{A}_{nm}|}, \tag{30}$$

where k is scale factor, and $|\hat{A}_{nm}^{(\gamma,k)}|$ and $|\hat{A}_{nm}|$ are the estimate magnitudes of the distorted image and original image, respectively. The proposed method does not require a scaling factor. Figure 11 shows the result of δA_{nm} between Figs. 6(a) and 6(c) for the proposed method ($k = 1$) and the direct method [k is calculated by Eq. (29)].

A measure to facilitate the comparison among different orthogonal moment calculations is by normalized mean squared error (NMSE), which is given as

$$\mathrm{NMSE}(|\hat{A}_{nm}|, |\hat{A}_{nm}^{(\gamma,k)}|) = \frac{1}{L^2}\sum_{n=1}^{L}\sum_{m=1}^{L}\frac{\left(\frac{1}{k^2}|\hat{A}_{nm}^{(\gamma,k)}| - |\hat{A}_{nm}|\right)^2}{|\hat{A}_{nm}|^2}, \tag{31}$$

where L^2 is the number of JFMs involved in the evaluation. Figure 12 shows the NMSE with angles of rotation of 2°–90°, with 4 intervals and scales of 0.75 and 0.5. For each rotation angle and scale, the first 100 JFMs ($L = 10$) are calculated with the proposed and direct method. It is clear that the proposed method greatly surpasses the direct method in terms of its invariance to rotation and scale. The NMSE values must be zero, but increase when the image is reduced and remain nearly constant when rotated.

C. Noisy Image Reconstruction

Sensitivity to noise is a critical issue for image moments. We compare the JFMs for peak signal to noise ratio (PSNR) and their performance for image reconstruction in the presence of noise. The PSNR is the ratio between a signal's maximum power and the power of the signal noise. PSNR is usually expressed in decibels, which is a logarithmic scale,

$$\mathrm{PSNR} = 10\log_{10}\left(\frac{255^2}{\mathrm{MSE}}\right). \tag{32}$$

Here, mean square error (MSE) is defined as

$$\mathrm{MSE} = \frac{1}{N\times M}\sum_{i=0}^{N-1}\sum_{j=0}^{M-1}(f(i,j) - f^*(i,j))^2, \tag{33}$$

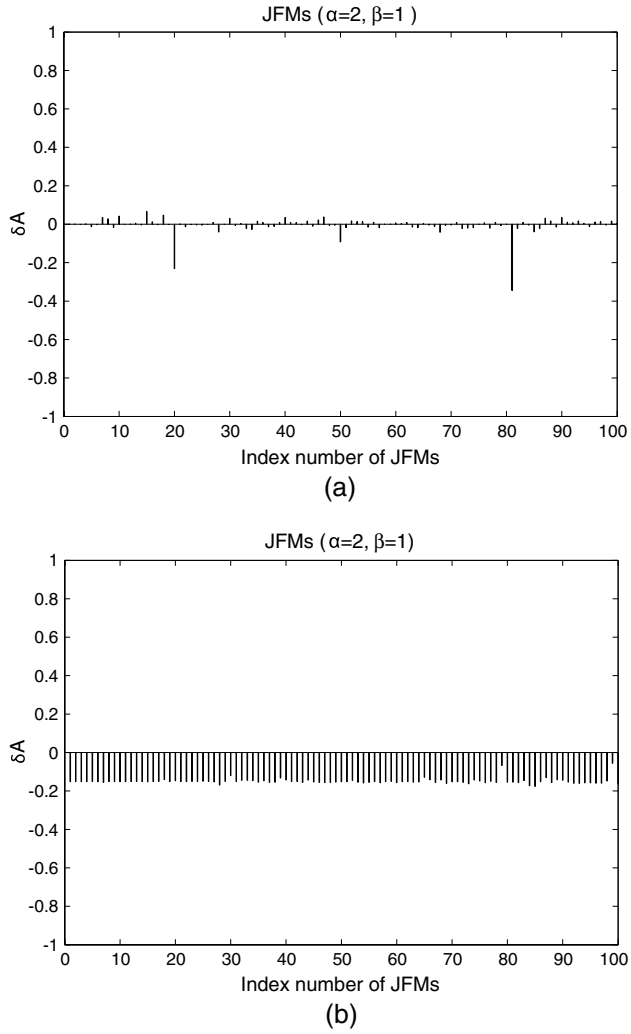

Fig. 11. Relative error between the first 100 JFMs of Figs. 6(a) and 6(c). (a) Results from the proposed method. (b) Results from the direct method.

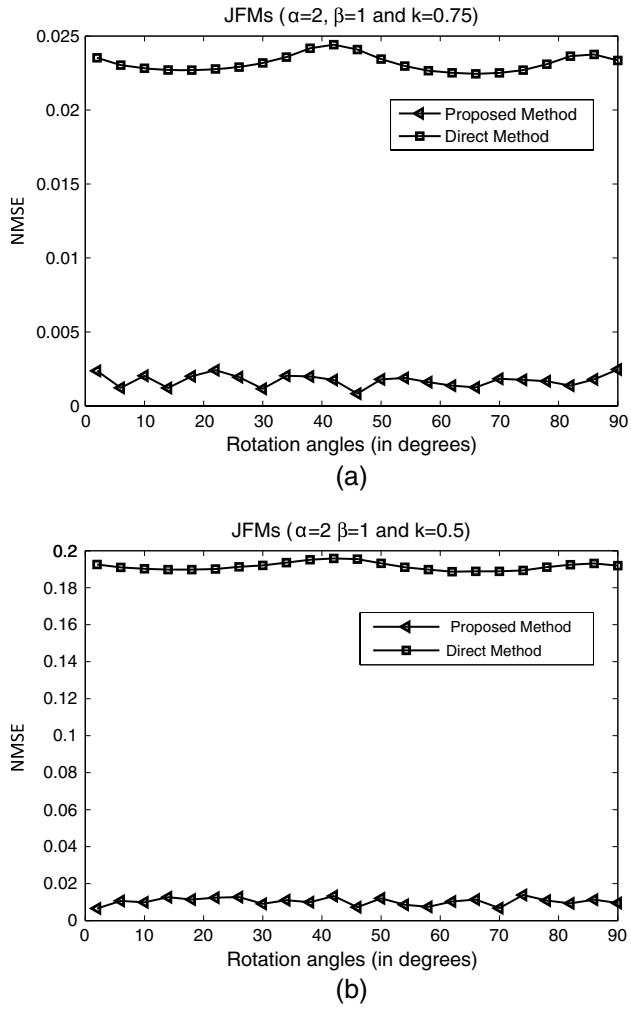

Fig. 12. NMSE for different scales. (a) Error calculated between Figs. 6(a) and 6(b). (b) Error computed between Figs. 6(a) and 6(d).

where $f(i,j)$ is the input image and $f^*(i,j)$ is the reconstruction of the noisy image. Figure 13 shows the result of PSNR of the boat image with different parameters of Gaussian noise ($\mu = 0$, $\sigma^2 = 0$, 0.02, 0.05, 0.1) using the proposed method, with $\alpha = 8$ and $\beta = 2$. The PSNR values decrease with increasing σ^2, and these changes are not very large for low-order moments ($L \leq 20$).

Moreover, the best PSNR values are when $L = 78$; the reconstruction is shown in Fig. 14. The results show that with higher-order moments than 20, the reconstruction is not reliable because the added noise degrades the reconstructed image.

D. Comparisons with Other Existing Algorithms

There are limited references on the fast and accurate calculation of the JFMs, although they have been the basis for generating new sets of orthogonal moments. However, in recent years, there has been some interest in the fast and accurate calculation of the OFMMs [18–20]. They have also been shown to be superior to other functions such as radial ZMs, particularly in terms of signal to noise ratio and reconstruction errors [6]. For these reasons, we performed a comparative analysis of the proposed method of JFMs with $\alpha = \beta = 2$ (OFMMs) versus the fast and accurate algorithms of the OFMMs. We performed a comparative analysis of the methods of Papakostas *et al.* [18], Hosny *et al.* [19], Walia *et al.* [20], and the direct calculation in terms of speed and accuracy for a 256×256 pixel image. Table 2 presents the computational complexity of the four methods. The comparison shows that,

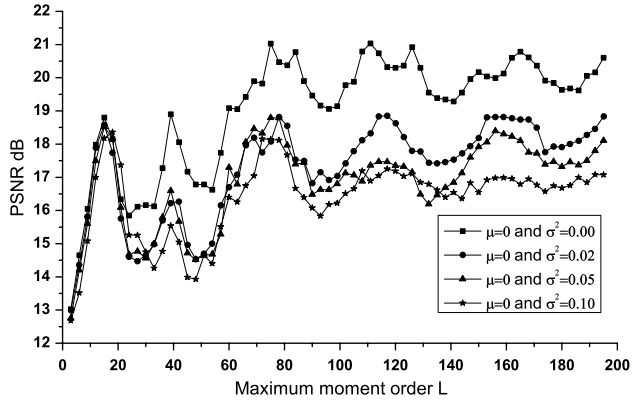

Fig. 13. PSNR of the 256×256 pixel reconstruction of the boat image, corrupted by an additive Gaussian noise of zero mean and $\sigma^2 = 0$, 0.02, 0.05, 0.01.

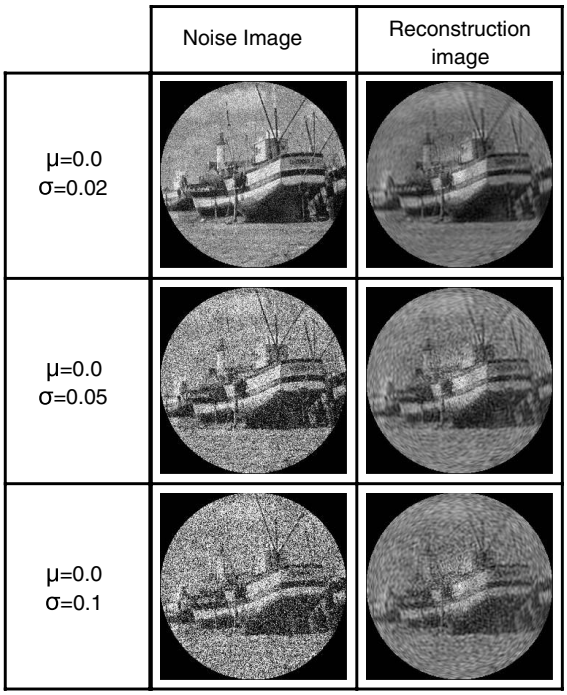

Fig. 14. Boat image corrupted by an additive Gaussian noise of zero mean and $\sigma^2 = 0.02, 0.05, 0.01$ and its respective reconstruction, with $L = 78$, $\alpha = 8$, and $\beta = 2$.

in the proposed method, the number of multiplications and additions is drastically reduced. Since the computation time does not depend on image content, only one image is considered for the analysis. To perform the simulations, a Sony Electronics, Inc., Model VAIO Computer Notebook PC with Intel Core i5-2430M CPU, 2.40 GHz processor, and 4.00 GB of RAM is used. The code is implemented using Matlab. Figure 15 shows the computation time of the different methods; as can be observed, the proposed method and the method of

Table 2. Comparison of Computations by Method

	Number of Additions	Number of Multiplications
Direct method	$\approx N^2(L^2+L)$ $+L(L+1)(L+2)$ $\left(\frac{8+N^2}{6}\right)$	$\approx 3N^2(L^2+L)$ $+L(L+1)(L+2)$ $\left(\frac{5+N^2}{6}\right)$
$N = 256$, $L = 10$	21628640	36045900
Papakostas *et al.* [18]	$\approx N^2(L^2+L)$ $+L(L+1)(L+2)$ $\left(\frac{5+N^2}{6}\right)$	$\approx N^2(3L^2+2L)$ $+L(L+1)(L+2)$ $\left(\frac{5+N^2}{6}\right)$
$N = 256$, $L = 10$	21627980	35390540
Hosny *et al.* [19]	$\approx N^2(L^2+3L)$ $+L(L+1)(L+2)$ $\left(1+\frac{N}{2}\right)$	$\approx N^2(3L^2+2L)$ $+L(L+1)(L+2)$ $\left(1+\frac{N}{3}\right)$
	8689960	21085480
Walia *et al.* [20]	$\approx N^2(L^2+3L)$	$\approx N^2(3L^2+5L)$
$N = 256$, $L = 10$	8519680	22937600
Our method	$\approx N^2(L^2+3L)$	$\approx N^2(3L^2+2L)+(L-2)$
(Proposed method)	$+(L-2)(16+N)$	$\left(10+\frac{3N}{2}\right)+N(31+L)$
$N = 256$, $L = 10$	8521856	20987728

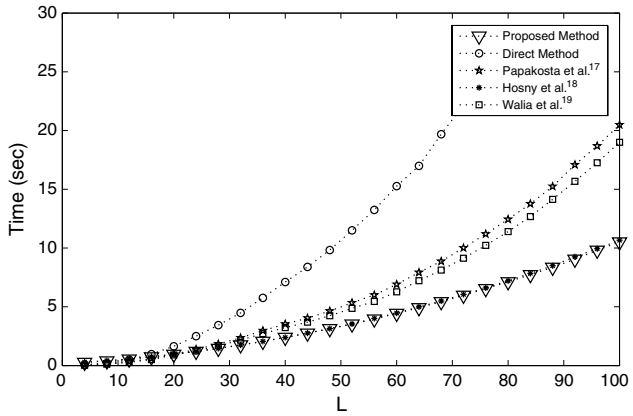

Fig. 15. Computing times for different methods with a 256×256 pixel image.

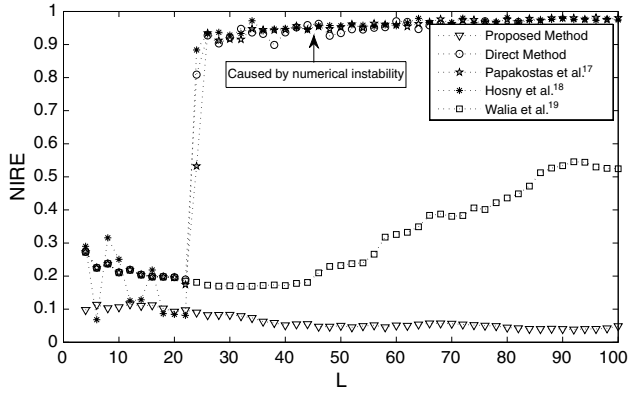

Fig. 16. Computation of NIRE for different methods with a 256×256 pixel image.

Hosny *et al.* are faster than the other methods. This is because using an arrangement of polar pixels facilitates the calculation of orthogonal moments. Although the Papakostas *et al.* and Walia *et al.* methods used recurrence relations that are faster than the direct method, these methods are based on square pixels.

The methods of Papakostas *et al.*, Hosny *et al.*, and the direct method are based on the calculation of the coefficients of Mellin orthogonal polynomials, which causes numerical instability for orders greater than 21, as can be observed in terms of NIRE as shown in Fig. 16. We can also observe that the methods based on recurrence relations with respect to n, such as our method and the Walia *et al.* method, are numerically stable. The Hosny *et al.* [19] method has a better image reconstruction for low orders due to its integration analytically, but is numerically unstable for high orders. It is clear that the proposed method is more precise and numerically stable than the compared methods.

6. CONCLUSIONS

We have proposed a novel approach for high-precision, fast computation of JFMs. Furthermore, this approach allows us to generate sets of different orthogonal moments. Ping *et al.* [1] suggest that the common formulation of the orthogonal moments through the Jacobi polynomials will be a benefit for performance analysis of the orthogonal moments and for searching a prime orthogonal moment. This idea has been

ignored due to its high computational costs. Our method facilitates the search of optimal parameters that best fit specific applications.

Moreover, improving the rotation and scale invariance compared to the direct method also facilitates the calculation because calculation of a scale factor is not required. The arrangement of polar pixels used and the proposed recurrence relation improves computation time and reconstruction error for gray-level images with large size. The numerical stability and accuracy of our method is proved through the NIRE, as shown in Fig. 9. It also has a higher numerical stability than the Xin *et al.* [14] method, as it is free of factorials and power of r, allowing for the computation of higher orders.

Experimental results show that the proposed method in this work performs consistently better than the methods of Papakostas *et al.*, Hosny *et al.*, Walia *et al.*, and the direct method in terms of image reconstruction capability and computation time for the OFMMs (JFMs with $\alpha = 2$ and $\beta = 2$). Therefore, the proposed method is not only faster, but is also high precision and numerically stable. It has direct applications in pattern recognition problems where invariant feature vectors are needed.

APPENDIX A: ZERNIKE MOMENTS

In Appendix B of [28], the relationship between Jacobi polynomials with the Zernike polynomials is given by

$$R^m_{m+2s}(r) = r^m J_s(m+1, m+1, r^2), \tag{A1}$$

where $R^m_{m+2s}(r)$ are the Zernike polynomials. Therefore, the coefficients C_s and D_s of Eq. (10), when $\alpha = \beta = m+1$, can be calculated as follows:

$$C_s = \frac{m^2}{(2s+m)(2s+m-2)}, \tag{A2}$$

$$D_s = \frac{2s(s+m)}{(2s+m)\sqrt{(2s+m+1)(2s+m-1)}}. \tag{A3}$$

For the initial calculation, the Jacobi polynomials of zeroth order and first order normalized in terms of the Zernike polynomials are given by

$$J_0(m+1, m+1, r^2) = 1, \tag{A4}$$

$$J_1(m+1, m+1, r^2) = -\sqrt{\frac{m+3}{m+1}}r^2. \tag{A5}$$

As seen, one can calculate a relation of recurrence of Zernike polynomials as a special case of the Jacobi polynomials. Furthermore, the ZMs cannot be calculated as a special case of the JFMs changing the parameters α and β, as mentioned in [1]. To check that it is not a special case, we have the JFMs, given by

$$\mathrm{JFM}^{\alpha,\beta}_{n,m} = \int_0^{2\pi}\int_0^1 f(r,\theta) J_n(\alpha,\beta,r) e^{-i\theta m}\mathrm{d}r\mathrm{d}\theta, \tag{A6}$$

where $J_n(\alpha,\beta,r)$ are the Jacobi polynomials. The ZMs are given as

$$\mathrm{ZM}_{n,m} = \int_0^{2\pi}\int_0^1 f(r,\theta) R^m_n(r) e^{-i\theta m}\mathrm{d}r\mathrm{d}\theta, \tag{A7}$$

where $R^m_n(r)$ are the Zernike polynomials. With the relationship between Eqs. (A1) and (A7) are obtained the $\mathrm{ZM}_{n,m}$ in terms of the Jacobi polynomials,

$$\mathrm{ZM}_{m+2s,m} = \int_0^{2\pi}\int_0^1 f(r,\theta) r^m J_s(m+1, m+1, r^2) e^{-i\theta m}\mathrm{d}r\mathrm{d}\theta. \tag{A8}$$

The JFMs when $\alpha = \beta = m+1$ and $n = s$ are given as

$$\mathrm{FM}^{m+1,m+1}_{s,m} = \int_0^{2\pi}\int_0^1 f(r,\theta) J_s(m+1, m+1, r) e^{-i\theta m}\mathrm{d}r\mathrm{d}\theta, \tag{A9}$$

and therefore $\mathrm{ZM}_{m+2s,m} \neq \mathrm{FM}^{m+1,m+1}_{s,m}$. The kernel of the ZMs has a different nature because angular order m is both in radial and angular coordinates, unlike JFM, which is only the angular coordinate. Moreover, calculating the Zernike polynomials from the Jacobi polynomials for the ZMs is not difficult. However, the JFMs cannot compare with the ZMs because every one has different complexity. The radial kernel of the ZMs depends on the radial and angular order and therefore requires a greater amount of Zernike polynomials, unlike the JFMs, which only require the polynomials of the radial order. This means that the JFMs have less computing time than the ZMs.

ACKNOWLEDGMENTS

This work is funded by CONACyT, México. César Joel Camacho Bello would like to thank CONACyT for scholarship number 423493.

REFERENCES

1. Z. Ping, H. Ren, J. Zou, Y. Sheng, and W. Bo, "Generic orthogonal moments: Jacobi–Fourier moments for invariant image description," Pattern Recogn. **40**, 1245–1254 (2007).
2. N. V. S. Sree Rathna Lakshmi and C. Manoharan, "An automated system for classification of micro calcification in mammogram based on Jacobi moments," IJCTE **3**, 431–434 (2011).
3. C. Toxqui-Quitl, A. Padilla-Vivanco, and J. Baez-Rojas, "Classification of mechanical parts using an optical-digital system and the Jacobi–Fourier moments," Proc. SPIE **7389**, 738934 (2009).
4. C. Camacho-Bello, C. Toxqui-Quitl, and A. Padilla-Vivanco, "Gait recognition by Jacobi–Fourier moments," in *Frontiers in Optics/Laser Science XXVII*, OSA Technical Digest (Optical Society of America, 2011), paper JTuA19.
5. M. R. Teague, "Image analysis via the general theory of moments," J. Opt. Soc. Am. **70**, 920–930 (1980).
6. Y. L. Sheng and L. X. Shen, "Orthogonal Fourier–Mellin moments for invariant pattern recognition," J. Opt. Soc. Am. A **11**, 1748–1757 (1994).
7. G. Amu, S. Hasi, X. Yang, and Z. Ping, "Image analysis by pseudo-Jacobi (p=4, q=3)-Fourier moments," Appl. Opt. **43**, 2093–2101 (2004).
8. Z. L. Ping, R. G. Wu, and Y. L. Sheng, "Image description with Chebyshev–Fourier moments," J. Opt. Soc. Am. A **19**, 1748–1754 (2002).
9. B. Xiao, J. F. Ma, and X. Wang, "Image analysis by Bessel–Fourier moments," Pattern Recogn. **43**, 2620–2629 (2010).
10. H. Ren, Z. Ping, W. Bo, W. Wu, and Y. Sheng, "Multi-distorted invariant image recognition with radial-harmonic-Fourier moments," J. Opt. Soc. Am. A **20**, 631–637 (2003).

11. H. Hu and P. Zi-liang, "Computation of orthogonal Fourier–Mellin moments in two coordinate systems," J. Opt. Soc. Am. A **26**, 1080–1084 (2009).
12. A. Padilla-Vivanco, G. Urcid-Serrano, F. Granados-Agustín, and A. Cornejo-Rodríguez, "Comparative analysis of pattern reconstruction using orthogonal moments," Opt. Eng. **46**, 017002 (2007).
13. S. X. Liao and M. Pawlak, "On the accuracy of Zernike moments for image analysis," IEEE Trans. Pattern Anal. Mach. Intell. **20**, 1358–1364 (1998).
14. Y. Xin, M. Pawlak, and S. Liao, "Accurate computation of Zernike moments in polar coordinates," IEEE Trans. Image Process. **16**, 581–587 (2007).
15. C. Y. Wee and R. Paramesran, "On the computational aspects of Zernike moments," Image Vis. Comput. **25**, 967–980 (2007).
16. R. Biswas and S. Biswas, "Polar Zernike moments and rotational invariance," Opt. Eng. **51**, 087204 (2012).
17. R. Mukundan and K. R. Ramakrishnan, "Fast computation of Legendre and Zernike moments," Pattern Recogn. **28**, 1433–1442 (1995).
18. G. A. Papakostas, Y. S. Boutalis, D. A. Karras, and B. G. Mertzios, "Fast numerically stable computation of orthogonal Fourier–Mellin moments," IET Comput. Vis. **1**, 11–16 (2007).
19. K. M. Hosny, M. A. Shouman, and H. M. Abdel Salam, "Fast computation of orthogonal Fourier–Mellin moments in polar coordinates," J. Real-Time Image Process. **6**, 73–80 (2011).
20. E. Walia, C. Singh, and A. Goyal, "On the fast computation of orthogonal Fourier–Mellin moments with improved numerical stability," J. Real-Time Image Process. **7**, 247–256 (2012).
21. M. Abramowitz and I. A. Stegun, *Handbook of Functions with Formulas, Graphs and Mathematical Tables* (Dover, 1964).
22. T. Hoang and S. Tabbone, "Errata and comments on 'generic orthogonal moments: Jacobi–Fourier moments for invariant image description," Pattern Recogn. **46**, 3148–3155 (2013).
23. C. Singh and R. Upneja, "Accurate computation of orthogonal Fourier–Mellin moments," J. Math. Imaging Vision **44**, 411–431 (2012).
24. C. Singh, E. Walia, and R. Upneja, "Accurate calculation of Zernike moments," Inf. Sci. **233**, 255–275 (2013).
25. R. G. Keys, "Cubic convolution interpolation for digital image processing," IEEE Trans. Acoust. Speech Signal Process. **29**, 1153–1160 (1981).
26. C. Toxqui-Quitl, L. Gutierrez-Lazcano, A. Padilla-Vivanco, and C. Camacho-Bello, "Gray-level image reconstruction using Bessel–Fourier moments," Proc. SPIE **8011**, 80112T (2011).
27. A. B. Bhatia and E. Wolf, "On the circular polynomials of Zernike and related orthogonal sets," Proc. Cambridge Philos. Soc. **50**, 40–48 (1954).
28. M. Born and E. Wolf, *Principles of Optics* (Cambridge University, 1999).